

[Supporting Information]

Particle Phase State and Aerosol Liquid Water Greatly Impact Secondary Aerosol Formation: Insights into Phase Transition and Role in Haze Events

Xiangxinyue Meng¹, Zhijun Wu^{1,2*}, Jingchuan Chen¹, Yanting Qiu¹, Taomou Zong¹, Mijung Song³, Jiye Lee⁴, Min Hu^{1,2}

1 State Key Joint Laboratory of Environmental Simulation and Pollution Control, International Joint Laboratory for Regional Pollution Control, College of Environmental Sciences and Engineering, Peking University, Beijing 100871, China

2 Collaborative Innovation Center of Atmospheric Environment and Equipment Technology, Nanjing University of Information Science and Technology, Nanjing 210044, China

3 Department of Earth and Environmental Sciences, Jeonbuk National University, Jeonju, Republic of Korea, 54896

4 Department of Environmental Science and Engineering, Ewha Womans University, Seoul, Republic of Korea, 03760

**Corresponding author: zhijunwu@pku.edu.cn*

Text S1. Detailed information of instruments equipped in the air monitoring laboratory

In this study, a weather station (Met One Instruments Inc., USA) was equipped in the laboratory to measure meteorological parameters, including ambient relative humidity (RH), temperature (T), wind speed (WS) and wind direction (WD). Trace gases were recorded using a suite of automatic gas analyzers from Thermo Scientific, including O₃ (model 49i), SO₂ (model 43i), CO (model 48i), and NO_x (model 42i). The chemical compositions of non-refractory particles

(NR-PM₁) were measured by Aerodyne Quadrupole Aerosol Chemical Speciation Monitor (Q-ACSM) equipped with a standard vaporizer. A perma pure nafion dryer was set up in front of the inlet of Q-ACSM to guarantee the RH below 30%. The instrument calibration was operated using pure ammonium nitrate and ammonium sulfate before and after the whole observation to determine the relative ionization efficiency followed by the standard protocols (Ng et al., 2011).

Figure S1. Time series and mass spectral profiles for PMF solution

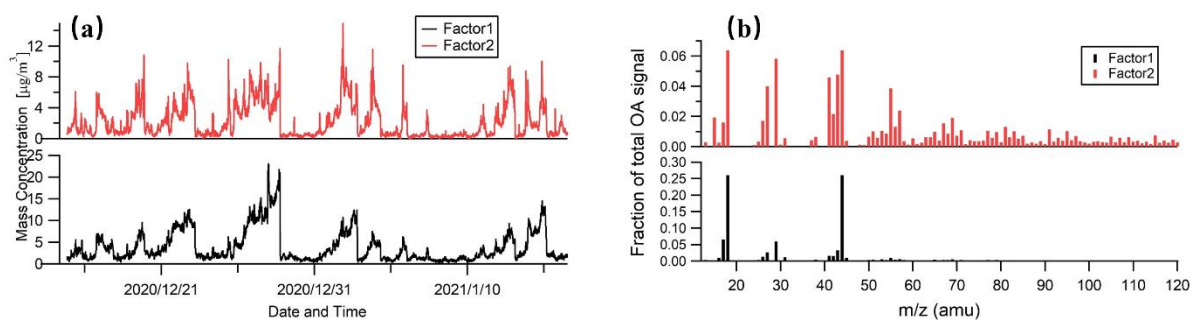


Figure S1. Time series (a) and mass spectral (b) profiles for the 2-factor PMF solution in PM₁. Factor 1 and factor 2 represent POA and SOA, respectively.

Figure S2. Summary of key diagnostic plots of the Q-ACSM PMF results for 2-factor resolution

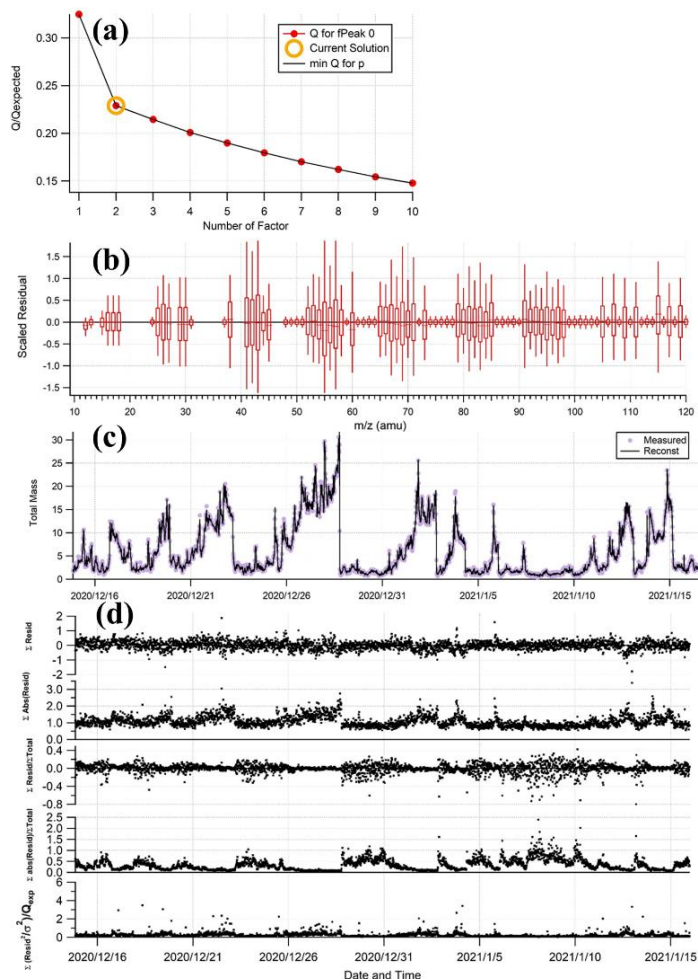


Figure S2. Summary of key diagnostic plots of the Q-ACSM PMF results for 2-factor resolution: (a) Q/Q_{exp} as a function of number of factors selected for PMF modeling. (b) the box and whiskers plot representing the distribution of OA scaled residuals for each m/z in selected mass spectra. (c) time series of the measured organic mass and the reconstructed OA mass (=POA+SOA). (d) time series of the residual diagnostics and Q/Q_{exp} for each point in time.

Figure S3. Contribution of organics to total aerosol liquid water content (ALWC)

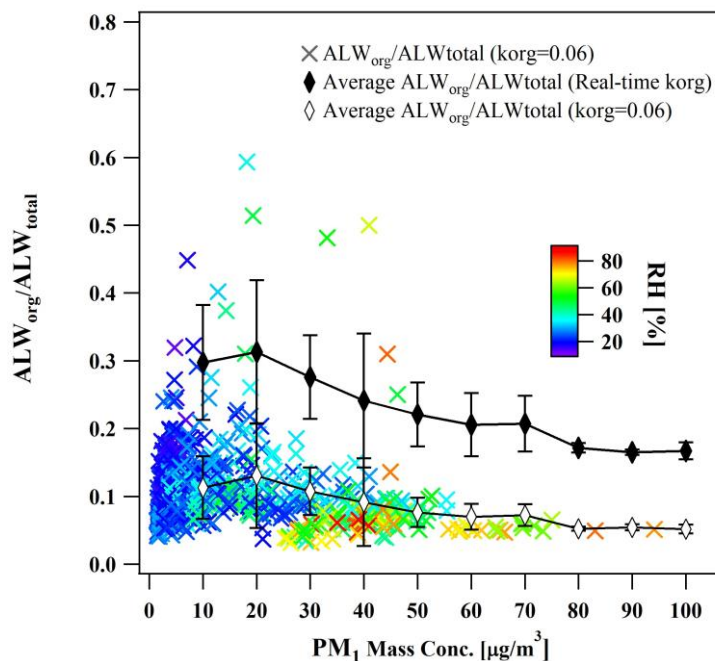


Figure S3. The colored scatter points represent the mass fraction of ALWC contributed by organics to total ALWC versus the PM_1 mass concentration, which was calculated by mean value of $k_{org}=0.06$. The color bar represents the ambient RH. The black line with solid and hollow points represents the contribution of average ALWC contributed by organics in total ALWC, which was calculated using average real-time k_{org} and fixed k_{org} .

Text S2. The unignorable contribution of organics to total ALWC

In this study, the real-time k_{org} was calculated as well with a wide range of f_{44} , which was widely used to represent the atmospheric aging process of OA species (Ng et al., 2010; Canagaratna et al., 2015). In Figure S3, we considered the variation of real-time f_{44} and calculated the real-time k_{org} to compare the difference on the mass contribution of organics to total ALW between fixed k_{org} and changing k_{org} . $k_{org}=0.06$ used in this study was lower than the commonly used $k_{org}=0.1$ in other studies (Gysel et al., 2007a), but was comparable with the retrieved k_{org} in Beijing varies in the range of 0.06-0.3 (Li et al., 2019; Jin et al., 2020). For fixed k_{org} , the contribution of organics to ALW was $\sim 12\%$ on average during the observation and organics

contributed more on clean days ($> 20\%$) than on polluted days ($< 10\%$). In general, organics with higher f_{44} exhibit larger hygroscopicity (Jimenez et al., 2009; Rickards et al., 2013). Though, the less hygroscopic nature of organics compared to inorganics, the significant fraction of organics to total aerosol mass have impact on total ALW mass. When considering the variation of real-time k_{org} of organics, organics contributed $\sim 29\%$ of the total ALW on average. Organics were capable to provide more than 30% and 20% of the total ALW mass on average during clean days and particulate pollution, respectively. It could be suggested that the increase of oxidation state of organics contributed the overall hygroscopicity of particles. Thus, the promoted hygroscopicity of particles under higher RH condition may increase the ALW mass and worsen the air quality. Even though the ALW calculations are different based on several methods (e.g. hygroscopicity tandem differential mobility analyzer (H-TDMA) measurements, the aerosol PNSD under dry and ambient RH conditions, chemical composition closure methods using Zdanovskii-Stokes-Robinson (ZSR) mixing rule and thermal equilibrium models such as ISORROPIA II model) (Kreidenweis and Asa-Awuku, 2014; Gysel et al., 2007b; Nguyen et al., 2016; Stanier et al., 2004), which may underestimate or overestimate the ALW contributed by organics (ALW_{org}), the mass fraction of ALW_{org} cannot be ignored irrespective of pollution level in winter Beijing.

Figure S4. Mass fraction of NR-PM₁ components

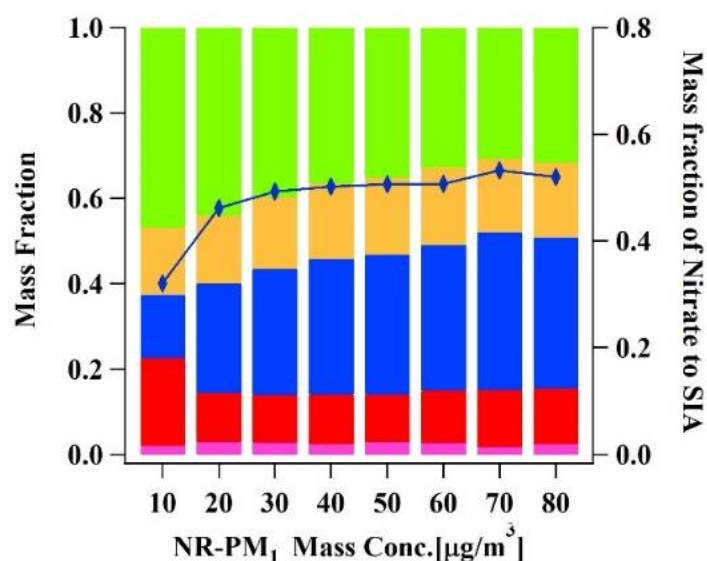


Figure S4. Mass fraction of NR-PM₁ composition and nitrate to SIA were grouped by the mass concentration of NR-PM₁.

Figure S5. Variation of average mass fraction of PM₁ components (NR- PM₁ and ALW) with PM₁ mass concentration

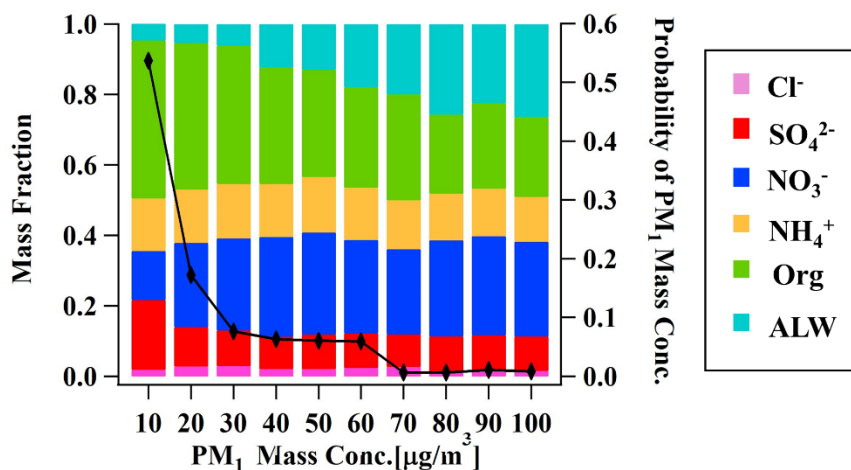


Figure S5. Variation of average mass fraction of NR-PM₁ and ALW with the PM₁ mass concentration and the probability of PM₁ mass concentration. The black line shows the probability of each PM₁ mass concentration bin.

Figure S6. Variation of organics components with PM₁ mass concentration

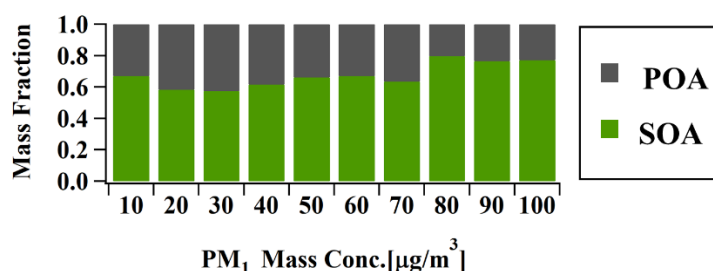


Figure S6. Variation of average mass fraction of POA and SOA with the increasing PM₁ mass concentration.

Text S3. Bulk phase viscosity of PM_{2.5} filter samples measured by Poke-and-flow experiments

Poke-and-flow experiments were conducted to determine the semi-solid or solid phases (non-liquid) of PM_{2.5} droplets during clean and polluted days at 293 ± 1 K (Gaikwad et al.,

2022;Renbaum-Wolff et al., 2013). As indicated by black and red frame with dashed lines in Figure 1f, filter samples on Dec 29, 2020 represented the clean day and the others (Dec 21 and 22, 2020 and Jan 1 and 2, 2021) represented the polluted days. Water-soluble species including inorganics and organics in the PM_{2.5} filter samples were extracted in purified water (18.2 MΩ·cm, Millipore, USA). Then, the PM_{2.5} droplets were nebulized on a hydrophobic substrate (Hampton Research, Canada) by a nebulizer and kept in a RH-controlled flow-cell (MEINHARD[®], Perkin Elmer, USA) for poke-and-flow experiments.

The procedures of the poke-and-flow experiments have been detailed in previous studies (Renbaum-Wolff et al., 2013;Jeong et al., 2022;Maclean et al., 2021b;Maclean et al., 2021a;Song et al., 2022). Briefly, the initial RH was set at ~100% so that droplets could reach equilibrium, and then the RH was reduced to ~40% at ~1% RH min⁻¹. Then, the droplets were poked at ~40%, ~30%, ~20%, ~10%, or ~0% RH by a needle (Jung Rim Medical Industrial, South Korea) to find the RH at which the droplets started to crack. Before each poking, the droplets were equilibrated for ~1 h at the setpoint RH. Once particles were cracked, they were monitored for ~3 h to check the occurrence of any inflow and outflow using a CCD camera (Hamamatsu, C11440-42U30, Japan). If no flow was detected, the lower limit of viscosity was defined as ~10⁸ Pa s (Grayson et al., 2015;Renbaum-Wolff et al., 2013;Song et al., 2019;Maclean et al., 2021b), corresponding to a (semi)solid state. It should be note that ~10⁸ Pa s was the lower limit of viscosity measurement for these PM_{2.5} filter samples by Poke-and-flow technique when no fluid was detected. Thus, (semi)solid, semisolid and liquid conditions were defined within the viscosity range of ~10⁸ Pa s, ~10⁸ Pa s to ~10² Pa s, and ~10² Pa s, respectively in this study. Although more precise values were not detected, we can still compare the particle rebound with viscosity range for these aerosols as shown in Figure S7 and Figure S8.

Figure S7. Comparison with online measured-particle rebound fraction and offline measured-viscosity by Poke-and-flow technique

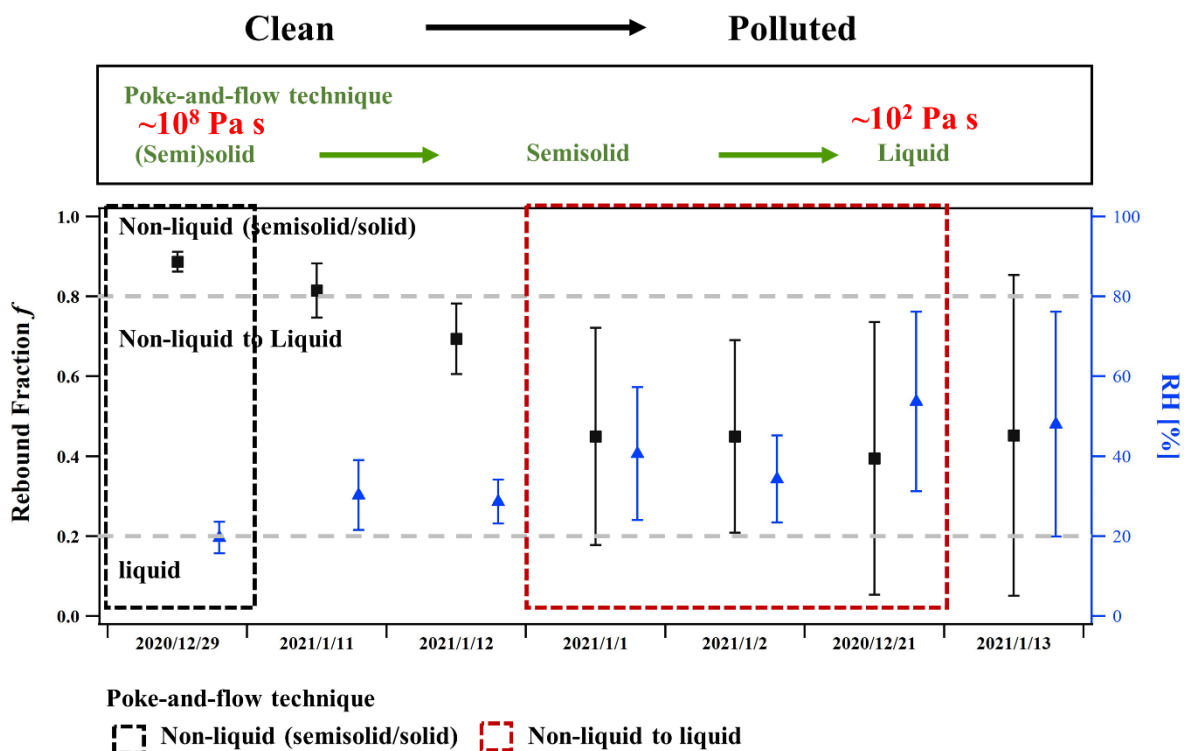


Figure S7. Averaged particle rebound fraction and ambient RH during filter sampling time for off-line viscosity measurement from clean to polluted days as reported in our previous study (Song et al., 2022). The black and red frames indicate clean day and polluted episodes, which are the same in Figure 1f. The viscosity results measured by Poke-and-flow technique are shown in the upper frame under certain ambient RH values (mean value of RH). Following our previous study, (semi)solid, semisolid, and liquid are defined as $\sim 10^8$ Pa s, $\sim 10^8 - \sim 10^2$ Pa s, and $\sim 10^2$ Pa s, respectively.

Figure S8. Correlation between particle rebound fraction and Poke-and-flow technique measurement for PM_{2.5} filter samples

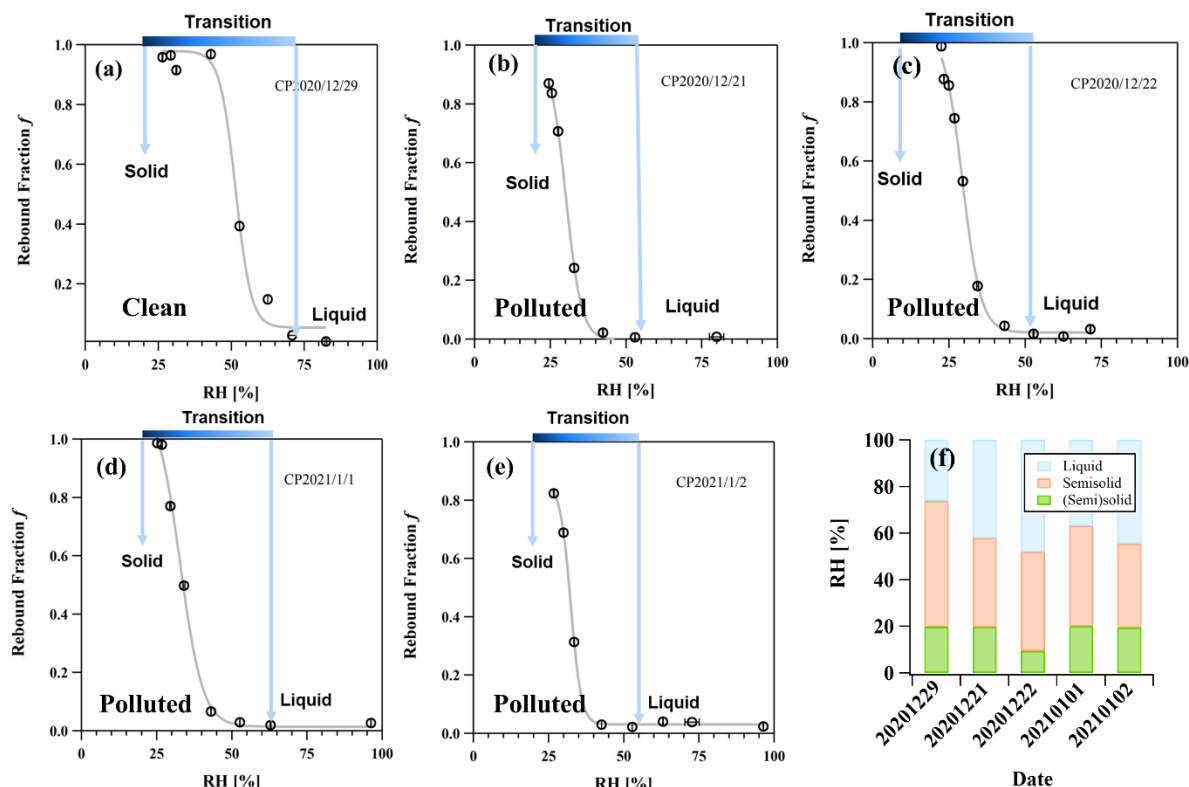


Figure S8. RH-dependent particle rebound fraction and viscosity range for PM_{2.5} filter samples during clean and polluted days as indicated in Figure 1f. In panel (f), the RH-dependent viscosity value was the same as our previous report (Song et al., 2022). In the rest panels, the colored blue bars indicate the corresponding RH ranges for the transition from (semi)solid to liquid based on Poke-and-flow technique. (semi)solid, semisolid, and liquid are defined as $\sim 10^8$ Pa s, $\sim 10^8 - \sim 10^2$ Pa s, and $\sim 10^2$ Pa s, respectively.

Text S4. Correlation between particle rebound fraction and Poke-and-flow technique measurement for PM_{2.5} filter samples

In order to demonstrate the viscosity variation of phase transition from non-liquid to liquid for the investigated aerosols, we conducted the tests on particle rebound fraction of extracted PM_{2.5} quartz-filter samples with known viscosity as reported above. We extracted these filter samples by the same protocols to get the water-soluble species followed by our previous study (Song et

al., 2022), and regenerated the aerosols by a commercial atomizer. Subsequently, the monodisperse aerosols were selected and directly sampled by the three-arm impactor to capture the particle rebound behavior. The particle rebound fraction were measured at decreasing RH levels from 90% to 20% at intervals of 10 min for each RH point, which mimicked the drying process for the determination of (semi)solid and solid phase measurement using the Poke-and-flow technique.

Figure S8 illustrates the viscosity range with corresponding RH conditions in panel (f), while the rested panels showed the RH-dependent particle rebound fraction of these aerosols. As indicated by black and red frame with dashed lines in Figure 1f, filter samples on Dec 29, 2020 represented the clean day and the others (Dec 21 and 22, 2020 and Jan 1 and 2, 2021) represented the polluted days. The blue bars indicate the corresponding RH range for (semi)solid to liquid phase transition, which was in the viscosity range of $\sim 10^8$ Pa s to $\sim 10^2$ Pa s. For filter samples on Dec 29, 2020, the ambient RH remained below 30% throughout the sampling period. We observed that particle rebound fraction was ~ 0.0 at RH = 70%, but steadily increased to ~ 1.0 as the RH decreased to $\sim 45\%$. Based on the detected RH value of (semi)solid for clean days ($\sim 20\%$), these particles were expected in a more viscous non-liquid state with particle rebound fraction higher than 0.8. For the filter samples on polluted days, the increased rebound fraction along with decreasing RH aligned well with the detected RH range for (semi)solid to liquid transition, indicating that particle rebound fraction with higher values (> 0.8) were expected to indicate the semi-solid or solid state, and phase transition from non-liquid to liquid could be directly inferred from the decreasing rebound fraction from >0.8 to ~ 0.0 . Although further detailed validation is still necessary to compare the two different techniques, both the online monitoring of particle rebound behavior during the campaign and the offline measurement of PM_{2.5} filter samples confirmed the consistent phase transition behavior during the polluted periods.

Figure S9. The variation of particle rebound fraction during changing RH from high to low conditions

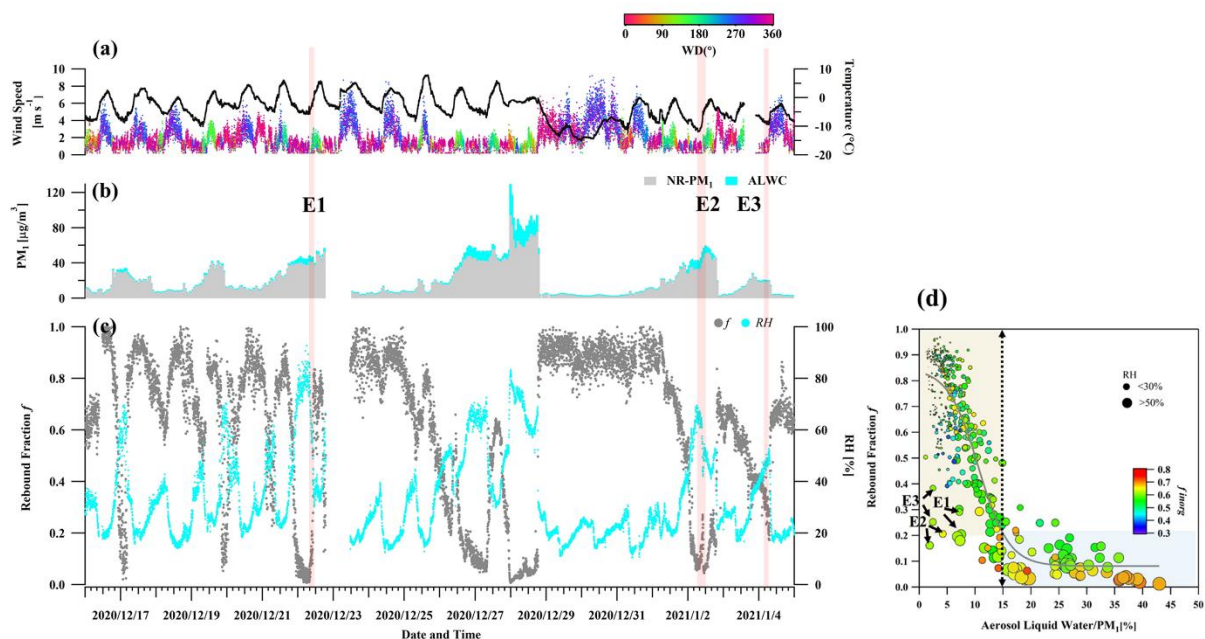


Figure S9. The variation of particle rebound fraction during changing RH from high to low conditions. Panel (a, b and c) were the same as those in Figure 1. Panel (d) was similar to Figure 2d, but particles with lower rebound fraction and ALW/NR-PM₁ < 5% were marked by E1, E2 and E3 with the black arrow and the corresponding periods were indicated by pink shadow in the time series of filed campaign as well.

Figure S10. SOA/POA as a function of rebound fraction during daytime and nighttime

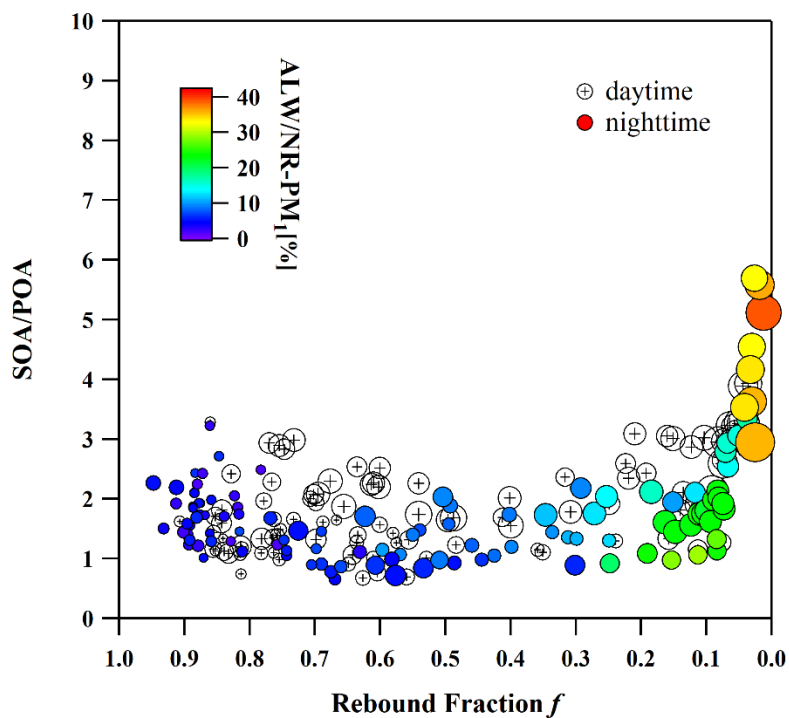


Figure S10. The relationship between SOA/POA and particle rebound fraction f for phase transition during the daytime (06:00-18:00) and nighttime (18:00-06:00+1 d). The points are colored by ALW/NR-PM₁ to represent the water uptake capacity of the particles. The NR-PM₁ mass concentration is indicated by the size of solid circles.

Figure S11. The hygroscopicity contributed by organics as a function of RH

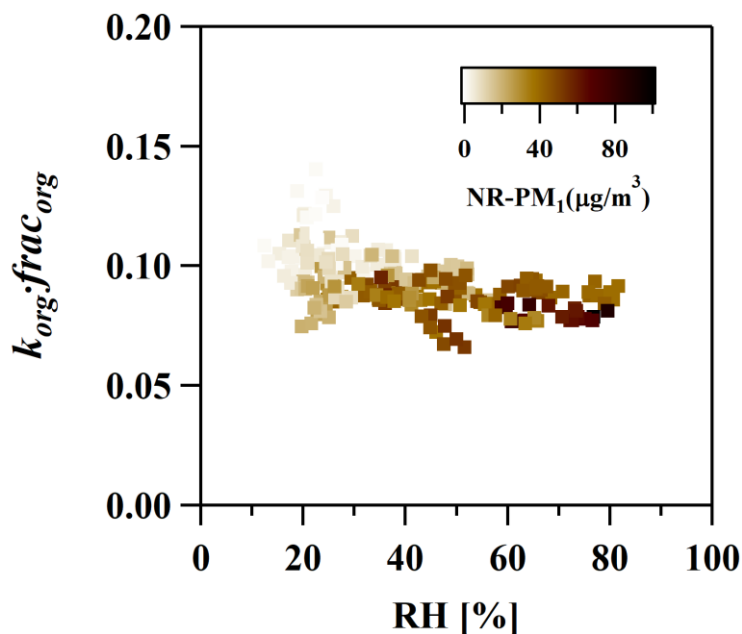


Figure S11. The hygroscopicity contributed by organics as a function of RH. The hygroscopicity of organics was calculated using real-time f_{44} measured by Q-ACSM. The color bar represents the NR-PM₁ mass concentrations.

Figure S12. Comparison of aerosol chemical composition, ambient conditions of RH and T, particle phase state and secondary transformation indicators of SIA and SOA for clean and polluted episodes

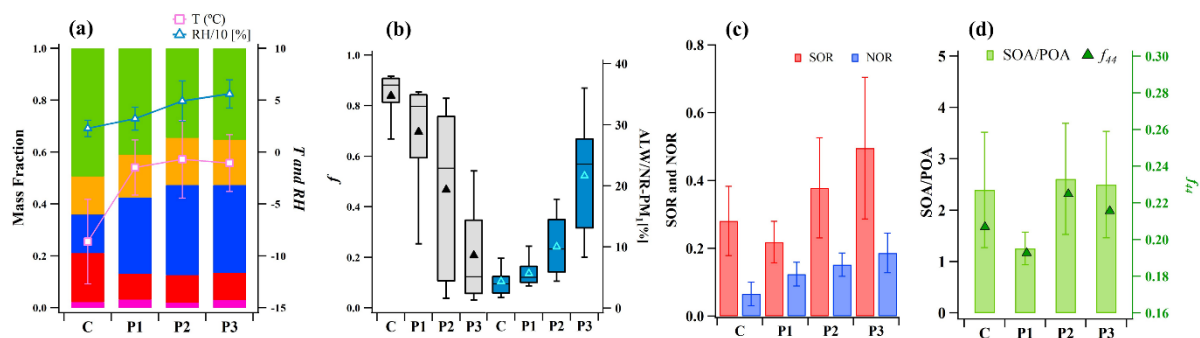


Figure S12. Changes of aerosol chemical composition, RH and T (a), f and ALW/NR-PM₁ (b), SOR and NOR (c), SOA/POA and f_{44} (d) for clean and polluted episodes (P1-P3). In panel (b), the box plots represent the 10th, 25th, 50th, 75th, and 90th percentiles of the corresponding

data. The solid and hollow triangle represents the mean value of the corresponding data for f and ALW/NR-PM₁, respectively.

Text S5. Case studies for polluted episodes during the field observation

Three polluted episodes (P1-P3) and one clean episode were investigated according to aerosol chemical composition, ambient conditions of RH and T, particle phase state and secondary transformation indicators of SIA and SOA. Overall, the polluted episodes had higher RH and T levels than the clean episodes, which favored the accumulation of ALW and associated multiphase processes. The enhanced mass fractions of SIA increased the particle water uptake capacity, leading to the phase transition during polluted episodes. However, phase transition from non-liquid to liquid occurred in P2 and P3 with $f = \sim 0.8-0.2$ and ALW/NR-PM₁ > 20% on average. These two polluted episodes had higher secondary transformation rates of SIA and SOA compared to the clean episode and P1 without phase transition, suggesting that phase transition may facilitate the secondary aerosol formation and the haze formation to a certain degree. It is therefore recommended that control strategies for gas pollutant emissions (e.g. SO₂ and NO_x) be implemented to effectively reduce air pollution in China.

Reference

- Canagaratna, M. R., Jimenez, J. L., Kroll, J. H., Chen, Q., Kessler, S. H., Massoli, P., Hildebrandt Ruiz, L., Fortner, E., Williams, L. R., Wilson, K. R., Surratt, J. D., Donahue, N. M., Jayne, J. T., and Worsnop, D. R.: Elemental ratio measurements of organic compounds using aerosol mass spectrometry: characterization, improved calibration, and implications, *Atmos. Chem. Phys.*, 15, 253-272, 10.5194/acp-15-253-2015, 2015.
- Gaikwad, S., Jeong, R., Kim, D., Lee, K., Jang, K.-S., Kim, C., and Song, M.: Microscopic observation of liquid-liquid-(semi)solid phases in polluted PM_{2.5}, *Front.*, 2022.
- Grayson, J. W., Song, M., Sellier, M., and Bertram, A. K.: Validation of the poke-flow technique combined with simulations of fluid flow for determining viscosities in samples with small volumes and high viscosities, *Atmos. Meas. Tech.*, 8, 2463-2472, 10.5194/amt-8-2463-2015, 2015.
- Gysel, M., Crosier, J., Topping, D. O., Whitehead, J. D., Bower, K. N., Cubison, M. J., Williams, P. I., Flynn, M. J., McFiggans, G. B., and Coe, H.: Closure study between chemical composition and hygroscopic growth of aerosol particles during TORCH2, *Atmos. Chem. Phys.*, 7, 6131-6144, 10.5194/acp-7-6131-2007, 2007a.
- Gysel, M., Crosier, J., Topping, D. O., Whitehead, J. D., Bower, K. N., Cubison, M. J., Williams, P. I., Flynn, M. J., McFiggans, G. B., and Coe, H.: Closure study between chemical composition and hygroscopic growth of

aerosol particles during TORCH2, *Atmos Chem Phys*, 7, 6131–6144, 2007b.

Jeong, R., Lilek, J., Zuend, A., Xu, R., Chan, M. N., Kim, D., Moon, H. G., and Song, M.: Viscosity and physical state of sucrose mixed with ammonium sulfate droplets, *Atmos. Chem. Phys.*, 22, 8805–8817, 10.5194/acp-22-8805-2022, 2022.

Jimenez, J. L., Canagaratna, M. R., Donahue, N. M., Prevot, A. S. H., Zhang, Q., Kroll, J. H., DeCarlo, P. F., Allan, J. D., Coe, H., Ng, N. L., Aiken, A. C., Docherty, K. S., Ulbrich, I. M., Grieshop, A. P., Robinson, A. L., Duplissy, J., Smith, J. D., Wilson, K. R., Lanz, V. A., Hueglin, C., Sun, Y. L., Tian, J., Laaksonen, A., Raatikainen, T., Rautiainen, J., Vaattovaara, P., Ehn, M., Kulmala, M., Tomlinson, J. M., Collins, D. R., Cubison, M. J., Dunlea, E. J., Huffman, J. A., Onasch, T. B., Alfarra, M. R., Williams, P. I., Bower, K., Kondo, Y., Schneider, J., Drewnick, F., Borrmann, S., Weimer, S., Demerjian, K., Salcedo, D., Cottrell, L., Griffin, R., Takami, A., Miyoshi, T., Hatakeyama, S., Shimojo, A., Sun, J. Y., Zhang, Y. M., Dzepina, K., Kimmel, J. R., Sueper, D., Jayne, J. T., Herndon, S. C., Trimborn, A. M., Williams, L. R., Wood, E. C., Middlebrook, A. M., Kolb, C. E., Baltensperger, U., and Worsnop, D. R.: Evolution of Organic Aerosols in the Atmosphere, *Science*, 326, 1525–1529, 2009.

Jin, X., Wang, Y., Li, Z., Zhang, F., Xu, W., Sun, Y., Fan, X., Chen, G., Wu, H., Ren, J., Wang, Q., and Cribb, M.: Significant contribution of organics to aerosol liquid water content in winter in Beijing, China, *Atmos. Chem. Phys.*, 20, 901–914, 10.5194/acp-20-901-2020, 2020.

Kreidenweis, S. M., and Asa-Awuku, A.: *Aerosol Hygroscopicity: Particle Water Content and Its Role in Atmospheric Processes*, 2014,

Li, X. X., Song, S. J., Zhou, W., Hao, J. M., Worsnop, D. R., and Jiang, J. K.: Interactions between aerosol organic components and liquid water content during haze episodes in Beijing, *Atmos. Chem. Phys.*, 19, 12163–12174, 2019.

Maclean, A. M., Li, Y., Crescenzo, G. V., Smith, N. R., Karydis, V. A., Tsimpidi, A. P., Butenhoff, C. L., Faiola, C. L., Lelieveld, J., and Nizkorodov, S. A.: Global Distribution of the Phase State and Mixing Times within Secondary Organic Aerosol Particles in the Troposphere Based on Room-Temperature Viscosity Measurements, *ACS Earth Space Chem*, 5, 3458–3473, 2021a.

Maclean, A. M., Smith, N. R., Li, Y., Huang, Y., Hettiyadura, A. P., Crescenzo, G. V., Shiraiwa, M., Laskin, A., Nizkorodov, S. A., and Bertram, A. K.: Humidity-Dependent Viscosity of Secondary Organic Aerosol from Ozonolysis of β -Caryophyllene: Measurements, Predictions, and Implications, *ACS Earth Space Chem*, 5, 305–318, 2021b.

Ng, N. L., Canagaratna, M. R., Zhang, Q., Jimenez, J. L., Tian, J., Ulbrich, I. M., Kroll, J. H., Docherty, K. S., Chhabra, P. S., Bahreini, R., Murphy, S. M., Seinfeld, J. H., Hildebrandt, L., Donahue, N. M., DeCarlo, P. F., Lanz, V. A., Prevot, A. S. H., Dinar, E., Rudich, Y., and Worsnop, D. R.: Organic aerosol components observed in Northern Hemispheric datasets from Aerosol Mass Spectrometry, *Atmos. Chem. Phys.*, 10, 4625–4641, 10.5194/acp-10-4625-2010, 2010.

Ng, N. L., Herndon, S. C., Trimborn, A., Canagaratna, M. R., Croteau, P. L., Onasch, T. B., Sueper, D., Worsnop, D. R., Zhang, Q., Sun, Y. L., and Jayne, J. T.: An Aerosol Chemical Speciation Monitor (ACSM) for Routine Monitoring of the Composition and Mass Concentrations of Ambient Aerosol, *Aerosol Sci. Technol.*, 45, 780–794, Pii 934555189
10.1080/02786826.2011.560211, 2011.

Nguyen, T. K. V., Zhang, Q., Jimenez, J. L., Pike, M., and Carlton, A. G.: Liquid Water: Ubiquitous Contributor to Aerosol Mass, *Environ. Sci. Technol. Lett.*, 3, 257–263, 2016.

Renbaum-Wolff, L., Grayson, J. W., Bateman, A. P., Kuwata, M., Sellier, M., Murray, B. J., Shilling, J. E., Martin,

S. T., and Bertram, A. K.: Viscosity of α -pinene secondary organic material and implications for particle growth and reactivity, *Proc. Natl. Acad. Sci.*, 110, 8014-8019, 2013.

Rickards, A. M. J., Miles, R. E. H., Davies, J. F., Marshall, F. H., and Reid, J. P.: Measurements of the Sensitivity of Aerosol Hygroscopicity and the κ Parameter to the O/C Ratio, *The Journal of Physical Chemistry A*, 117, 14120-14131, 10.1021/jp407991n, 2013.

Song, M., Maclean, A. M., Huang, Y., Smith, N. R., Blair, S. L., Laskin, J., Laskin, A., DeRieux, W.-S. W., Li, Y., Shiraiwa, M., Nizkorodov, S. A., and Bertram, A. K.: Liquid-liquid phase separation and viscosity within secondary organic aerosol generated from diesel fuel vapors, *Atmos. Chem. Phys.*, 19, 12515-12529, 10.5194/acp-19-12515-2019, 2019.

Song, M., Jeong, R., Kim, D., Qiu, Y., Meng, X., Wu, Z., Zuend, A., Ha, Y., Kim, C., Kim, H., Gaikwad, S., Jang, K.-S., Lee, J. Y., and Ahn, J.: Comparison of Phase States of PM_{2.5} over Megacities, Seoul and Beijing, and Their Implications on Particle Size Distribution, *Environ. Sci. Technol.*, 10.1021/acs.est.2c06377, 2022.

Stanier, C. O., Khlystov, A. Y., Chan, W. R., Mandiro, M., and Pandis, S. N.: A method for the in situ measurement of fine aerosol water content of ambient aerosols: The dry-ambient aerosol size spectrometer (DAASS), *Aerosol Science and Technology*, 38, 215-228, 2004.